Zinc enrichment and isotopic fractionation in a marine habitat of the c. 2.1 Ga Francevillian Group: A signature of zinc utilization by eukaryotes?

Frantz Ossa Ossa [a,b,c,d,*], Marie-Laure Pons [e,b], Andrey Bekker [f,d], Axel Hofmann [d], Simon W. Poulton [g], Morten B. Andersen [c], Andrea Agangi [h,d], Daniel Gregory [i], Christian Reinke [j], Bernd Steinhilber [b], Johanna Marin-Carbonne [k], Ronny Schoenberg [b,d]

[a] *Department of Earth Science, Khalifa University, P O Box 127788, Abu Dhabi, United Arab Emirates*
[b] *Department of Geosciences, University of Tuebingen, Schnarrenbergstrasse 94-96, 72076 Tuebingen, Germany*
[c] *School of Earth & Environmental Sciences, Cardiff University, Cardiff CF10 3AT, UK*
[d] *Department of Geology, University of Johannesburg, 2092 Johannesburg, South Africa*
[e] *CNRS, Aix Marseille Univ, IRD, INRA, Coll France, CEREGE, 13545, Aix en Provence, France*
[f] *Department of Earth and Planetary Sciences, University of California, Riverside, CA 92521, USA*
[g] *School of Earth and Environment, University of Leeds, Leeds LS2 9JT, UK*
[h] *Department of Earth Resource Science, Akita University, Akita 010-8502, Japan*
[i] *Department of Earth Sciences, University of Toronto, Toronto, Ontario M5S 3B1, Canada*
[j] *Spectrum Facilities, Faculty of Science, University of Johannesburg, 2092 Johannesburg, South Africa*
[k] *Institute of Earth Sciences (ISTE), University of Lausanne, 1015 Lausanne, Switzerland*

A R T I C L E   I N F O

A B S T R A C T

Constraining the timing of eukaryogenesis and the divergence of eukaryotic clades is a major challenge in evolutionary biology. Here, we present trace metal concentration and zinc isotope data for c. 2.1 billion-year-old Francevillian Group pyritized structures, previously described as putative remnants of the first colonial multicellular organisms, and their host black shales. Relative to the host rocks, pyritized structures are strongly enriched in zinc, cobalt and nickel, by at least one order of magnitude, with markedly lighter zinc isotope compositions. A metabolic demand for high concentrations of aqueous zinc, cobalt, and nickel combined with preferential uptake of lighter zinc isotopes may indicate metalloenzyme utilization by eukaryotes in marine habitats c. 2.1 billion years ago. Once confirmed, this would provide a critical calibration point for eukaryogenesis, suggesting that this major evolutionary innovation may have happened contemporaneously with elevated atmospheric oxygen levels during the latter part of the Great Oxidation Event, some 400 million years earlier than is currently widely accepted.

© 2023 The Author(s). Published by Elsevier B.V. This is an open access article under the CC BY license (http://creativecommons.org/licenses/by/4.0/).

1. Introduction

The evolution and early diversification of eukaryotes were defining moments in the history of life on Earth. However, despite considerable advances in phylogenetic and molecular clock estimates, a dearth of paleobiological signatures in the Precambrian sedimentary record, including fossils and molecular biomarkers, has strongly hampered attempts to track eukaryogenesis and the subsequent divergence of eukaryotic kingdoms. Purported eu-

karyotic affinity of pre-1.6 Gyr old fossils remains uncertain (e.g., Betts et al., 2018; Javaux, 2019). Moreover, while a precise age of *Bangiomorpha pubescens* suggests that the first unambiguous crown group of eukaryotes is as old as c. 1.05 Gyr (Gibson et al., 2018), more recent molecular clock models propose earlier estimates, sometime during the Mesoproterozoic (Porter, 2020). Furthermore, while fossil records suggest that eukaryotes did not diverge into their main lineages until c. 800 Ma ago (Butterfield, 2015; Javaux, 2019; Knoll, 2014), molecular clocks, in contrast, argue for much earlier diversification in the Meso- to early Neoproterozoic (Strassert et al., 2021). However, an estimate for eukaryote diversification based on fossils broadly coincides with the oldest preserved eukaryote-derived organic biomarkers (steranes) in the

* Corresponding author at: Department of Earth Science, Khalifa University, P O Box 127788, Abu Dhabi, United Arab Emirates.
E-mail address: frantz.ossaossa@ku.ac.ae (F. Ossa Ossa).

sedimentary record, which are constrained in age between c. 800 and 700 Ma (Brocks et al., 2017; Love et al., 2009; Summons et al., 1988; Zumberge et al., 2020).

Molecular clock models use the rate of mutations to estimate the timing and duration of divergence between species on a phylogenetic tree. The main approach in commonly used models, such as MULTIDIVTIME and Markov Chain Monte Carlo Tree (MCMC-TREE), consists of fixing one or more calibration/divergence points–nodes–based on fossil or geological records (e.g., organic and inorganic geochemistry) to estimate the timing of all other divergence points on the tree (e.g., Inoue et al., 2010 and references therein). Therefore, the accuracy of these estimates depends highly on the robustness of these calibration points. By contrast, the lack of unequivocal paleobiological signature for eukaryotes in older sedimentary rocks has led to considerable uncertainty in phylogenetic and molecular clock estimates for the emergence of the last eukaryote common ancestor (LECA), as well as uncertainty in terms of the time between the emergence of the LECA and the divergence of the main eukaryotic supergroups (Betts et al., 2018; Burki et al., 2020; Eme et al., 2014; Gold et al., 2017; Knoll, 2014; Parfrey et al., 2011; Porter, 2020; Strassert et al., 2021). For example, relaxed molecular clock methods, based on taxon-rich multigene data combined with diverse fossil evidence, estimate the emergence of LECA between c. 2.4 and 1.6 Gyrs ago (Betts et al., 2018; Parfrey et al., 2011; Porter, 2020; Strassert et al., 2021), which is broadly consistent with undisputed fossil evidence for eukaryotes at c. 1.6 Gyrs ago, respectively (Pang et al., 2013). Based on this approach, the divergence of the main eukaryote lineages is estimated to have occurred before 1 Gyrs ago (Parfrey et al., 2011; Strassert et al., 2021), which is considerably earlier than the most widely accepted fossil evidence (Javaux, 2019; Knoll, 2014; Love et al., 2009; Summons et al., 1988; Zumberge et al., 2020). By contrast, a molecular clock approach based on sterol biosynthesis, which is a characteristic eukaryote sterane biomarker, potentially links the emergence of the LECA to the Great Oxidation Event (GOE), c. 2.43 to 2.1 Gyrs ago (Gold et al., 2017). Although there is still large uncertainty on these estimates, placing the LECA between c. 3.1 and 1.7 Gyrs ago (Gold et al., 2017), a link between LECA and the GOE also overlaps with the Bayesian molecular clock approach under a scenario of serial endosymbiosis used by Strassert et al. (2021).

Many factors may explain the discrepancy in age estimates for eukaryogenesis, including the precise taxa and gene selected, the assumed phylogeny of eukaryotes, molecular clock methods, and the models used (Eme et al., 2014). However, the paucity of reliable calibration points due to the fragmentary nature of the fossil record has an overarching influence on this uncertainty (Eme et al., 2014; Gold et al., 2017; Parfrey et al., 2011). To address this issue, we focus on c. 2.1 Gyr old Francevillian Group pyritized structures previously described as fossils of a macroscopic population of probable colonial organisms (El Albani et al., 2010), and their host sediments. These putative multicellular organisms appear to have thrived in oxygenated marginal marine conditions (El Albani et al., 2010). However, although a eukaryote origin has been considered for these Francevillian Group putative fossils (El Albani et al., 2010), their biogenicity has been questioned (e.g., Anderson et al., 2016). Furthermore, if representing biological remnants, their affinity within the three main domains of life – archea, bacteria, and eukarya – is also uncertain (e.g., Nelson and Smith, 2019). Here, we utilize zinc concentrations [Zn] and isotopic compositions ($\delta^{66}Zn$; representing the $^{66}Zn/^{64}Zn$ ratio of the sample relative to the JMC-3-0749L reference standard), coupled with other metal concentrations (e.g., Co, Ni, Mn and Ag), to provide new insight into the biogenicity and biological affinity of these enigmatic Paleoproterozoic pyritic structures, which are henceforth termed as 'fossilized structures' to avoid implying a macro-faunal heritage.

2. Geological setting

The Francevillian Group is a c. 2.1 Gyr old Paleoproterozoic sedimentary succession in southeast Gabon that only experienced burial diagenesis, with maximum temperatures less than 120°C (El Albani et al., 2010; Ossa Ossa et al., 2013, 2022). It is developed in the c. 44,000 km^2 Francevillian basin, which is subdivided into 4 sub-basins, named the Boué (Plateau des Abeilles), Lastoursville, Franceville, and Okindja sub-basins (Fig. 1). The Francevillian Group is subdivided into five lithostratigraphic formations, from the Francevillian A (FA) at the bottom to Francevillian E (FE) at the top (El Albani et al., 2010; Gauthier-Lafaye and Weber, 2003; Ossa Ossa et al., 2013, 2018). The FA Formation consists of conglomerate, sandstone, and shale, recording the evolution of depositional environments from fluvial in its lower part to a tide-influenced fluvio-deltaic setting in the upper part (Gauthier-Lafaye and Weber, 2003). In the FB Formation, interbedded black shale, siltstone, sandstone, and carbonate indicate marine environments that fluctuated between intertidal and outer-shelf settings (El Albani et al., 2010; Gauthier-Lafaye and Weber, 2003; Ossa Ossa et al., 2013, 2018, 2022). The FC Formation is marked by the development of an extensive marine carbonate platform on an open shelf (Gauthier-Lafaye and Weber, 2003; Ossa Ossa et al., 2018). The FD to FE formations are characterized by marine black shales, with intercalations of sandstones, containing a significant contribution from submarine volcanic and subaerial volcaniclastic material (Gauthier-Lafaye and Weber, 2003).

The FB and lower part of the FC formations were deposited in an oxygenated, intertidal to outer shelf environment connected to the open ocean, and these formations record the c. 2.22-2.06 Gyr old Lomagundi Event (LE) (El Albani et al., 2010; Ossa Ossa et al., 2013, 2018, 2022). The LE is Earth's most pronounced and long-lived positive carbon isotope excursion, and is generally interpreted to reflect high primary productivity and organic carbon burial in the marine environment (Karhu and Holland, 1996). Although it has recently been suggested that the Lomagundi carbon isotope excursion was restricted to shallow-marine settings, with deep-marine environments being much less isotopically fractionated (Prave et al., 2021), a wide range of combined geochemical and sedimentological evidence challenges this interpretation and links the LE with oxygen build-up in the atmosphere-hydrosphere system during the later part of the GOE (e.g., Bekker et al., 2021; Karhu and Holland, 1996; Ossa Ossa et al., 2013, 2022). The unique feature of the FB Formation is that black shales host pyritized and non-pyritized macroscopic fossilized structures, which are possible remnants of marine organisms (El Albani et al., 2010, 2014, 2019). The symmetrical organization of the fossilized structures and the reproducibility of such complex morphologies, which were argued to be a unique trait for a biogenic origin, led previous studies to propose that these Francevillian Group macroscopic structures were fossilized multicellular organisms (El Albani et al., 2010, 2014). In contrast to the lower Francevillian stratigraphic units, the upper part of the FC Formation and the FD Formation were deposited under predominantly anoxic water column conditions and record the end of the LE (Ossa Ossa et al., 2018, 2022).

Our sample set spans the upper FA to lower FC formations (Fig. 1). The fossilized structures studied here are diverse in size and morphology (Figs. 2, S1). They were collected in two geographical locations ~12 km apart (Fig. 1). Most of these fossilized structures are pyritized as subrounded and subhedral pyrite grains together with an intra- and inter-granular carbonaceous matrix (Fig. S2; El Albani et al., 2010). The morphology of these specimens (Figs. 2, S1, S2), named here as Eyo, Ekang, Endama, Engong, and Aki, has been described previously and was interpreted to reflect putative large multicellular colonies with coordinated growth (El Albani et al., 2010, 2014, 2019). In particular, the Eyo speci-
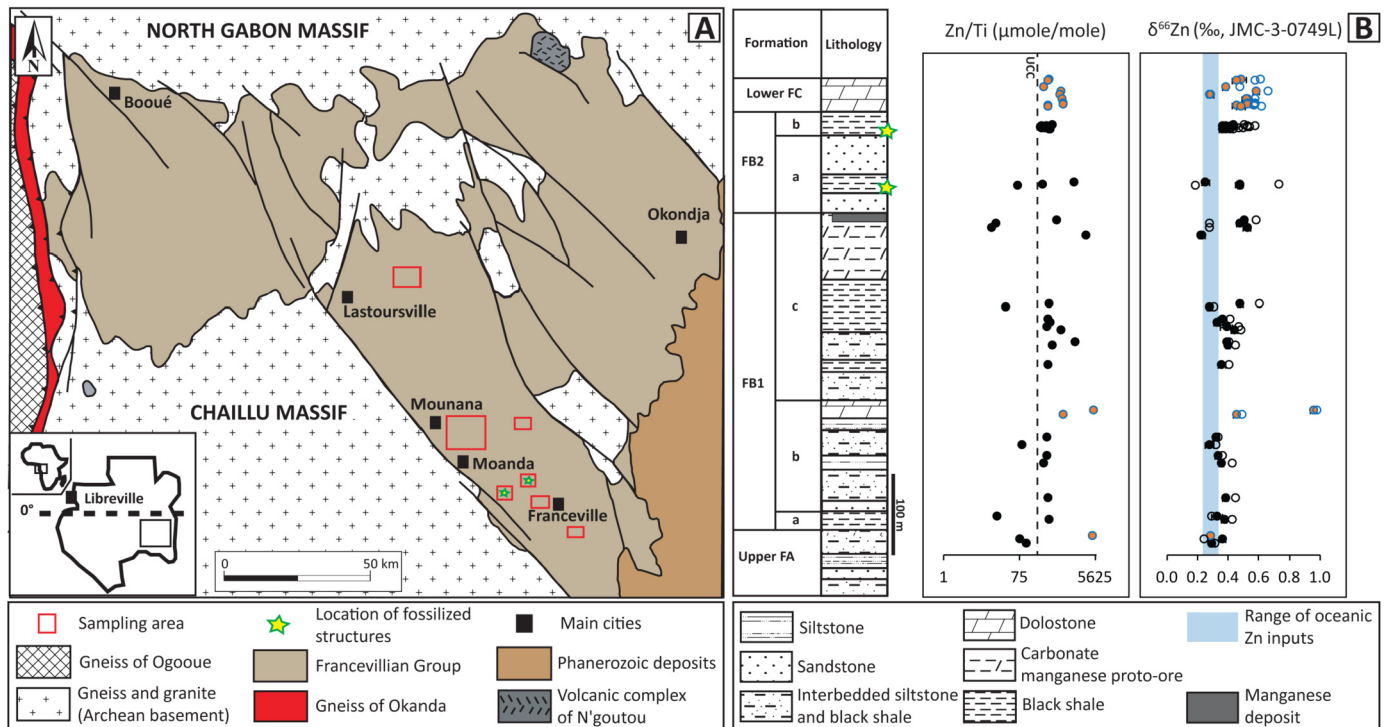
Fig. 1. A: Simplified geological map of the Francevillian basin showing sample locations. **B:** Lithostratigraphic profile and geochemical data for the Francevillian Group, including black shales (black-filled circles) and carbonates (orange-filled circles) from the upper FA to lower FC formations. Dashed line in Zn/Ti plot represents the average value for the upper continental crust (UCC) (Rudnick and Gao, 2014); the isotopic range of the main oceanic inputs in the δ^{66}Zn plot is from Little et al. (2014). Error bars on δ^{66}Zn values represent individual 2SE obtained during measurements (see Table S2). Empty circles in the δ^{66}Zn plot represent estimates for authigenic Zn isotope composition of shale (black empty circles) and seawater carbonates (blue empty circles) following Little et al. (2016). Due to uncertainty related to lithogenic Zn concentrations, this method to estimate authigenic component induces larger errors for shales (see Table S2) and therefore error bars are not shown for individual samples here to avoid cluttering. Since bulk carbonate δ^{66}Zn values corrected for lithogenic component yielded very small errors (Table S2), the overlapping high Zn isotope values for carbonates and shales are considered as conservative authigenic δ^{66}Zn values with a minimal error.

men (Figs. 2 and S1) has an elongated, sinuous shape and is tightly folded (El Albani et al., 2014); specimens Ekang, Endama, and Aki (Figs. 2, S1, S2) are similar to previously described lobate forms showing a sheet-like structure and radial fabric (El Albani et al., 2010, 2014), whereas Engong specimens (Fig. 2) have a weakly pyritized to non-pyritized discoidal shape with a flange-like outer part (El Albani et al., 2014). Sulfur isotope ratios show that pyritization of these fossilized structures, along with growth of diagenetic pyrite unrelated to these structures (such as concretions and disseminated grains) at the same stratigraphic level, occurred via microbial sulfate reduction during early diagenesis (El Albani et al., 2010, 2014, 2019; Ossa Ossa et al., 2018).

3. Results

Metal concentrations and Zn isotope compositions were investigated for the Francevillian Group fossilized structures, including pyritized and non-pyritized types, and their host rocks, black shales and carbonates (Figs. 1B, 3, 4, 5, S1-S3; Tables S1-S3). Microbial mat structures, diagenetic pyrite concretions unrelated to fossilized structures, thin pyrite beds formed at the water-sediment interface, and diagenetic carbonate concretions were also analyzed (Figs. 3, 4, 5, S4, Tables S1-S3). Geochemical and morphological features of these microbial mat structures were used to argue that their biomass was photosynthetically produced by cyanobacteria (Aubineau et al., 2018). In addition, for further geochemical comparison, c. 3.0 and 2.85 Gyr old continental and marine Archean diagenetic pyrites and their host black shales, as well as c. 183 million year (Myr) old Jurassic (Toarcian) diagenetic pyrite suns and their host black shales, were also analyzed (Figs. 5, S5, Tables S2). Pyrite suns are concretions that grew fast as discs and

flower petals through radial crack propagation in stiff mud during compaction. They are a common diagenetic feature that could be mistaken for pyritized fossils in bituminous shales (Seilacher, 2001). Analytical methods are detailed in the Supplementary Information.

Microtextural analyses using scanning electron microscope (SEM), electron probe microanalyzer (EPMA), and laser-ablation inductively coupled mass-spectrometry (LA-ICP-MS) techniques confirmed that fossilized structures and other Francevillian Group sulfides are dominantly composed of pyrite, with sulfur concentrations between 43 and 55 wt.%, and Fe concentrations between 45 and 47 wt.% (Fig. 3, Table S1). Sphalerite ((Zn,Fe)S) and galena (PbS) mineral phases are rare and occur in the rock matrix as disseminated grains or inclusions in diagenetic pyrite concretions unrelated to fossilized structures (Fig. 3). Zinc EPMA compositional maps of fossilized structures show c. 10 to 100 µm-sized subrounded and subhedral pyrite grains with thin Zn-enriched rims, whereas Co, also associated with these pyrite grains, shows no apparent distribution pattern (Fig. 3).

Bulk analyses of 20 to 50 mg of powders obtained from microdrilled pyritized and non-pyritized Francevillian Group fossilized structures show [Zn] between 142 and 835 µg/g, [Co] between 345 and 1255 µg/g, and [Ni] between 451 and 2925 µg/g, whereas the same amount of powder from the host shales yields lower [Zn] between 67 and 126 µg/g, [Co] between 0.75 and 184 µg/g, and [Ni] between 6 and 305 µg/g (Table S2). While both host rocks and fossilized structures have, on average, Zn, Co, and Ni concentrations above those of the upper continental crust (UCC) (67, 17.3, and 47 µg/g, respectively; Rudnick and Gao, 2014), concentrations in the fossilized structures are several times higher than those of the host rocks. Metal concentrations always appear to be correlated

Fig. 2. Francevillian fossilized structures. Photo images of representative specimens of the Francevillian Group fossilized structures and/or their imprints, including Eyo, Ekang, Endama, and Engong, as well as the host sediments showing their respective [Zn] and δ^{66}Zn values. Fossilized structures are characterized by higher [Zn] and lower δ^{66}Zn values compared to their host sediments. Morphology of similar fossilized structures has previously been described in detail (El Albani et al., 2010, 2014, 2019). Scale bar is 2 cm and white stars point to analyzed portions of the samples for Zn concentration and isotope composition.

with the size of the structure, with the largest fossilized structures yielding the highest enrichments (Fig. 2). These Zn, Co, and Ni concentrations in pyritized and non-pyritized structures are also much higher than those in the Francevillian Group microbial mat structures as well as all the other comparative material investigated (Figs. 4, 5A, 5B; Tables S1, S2). Similarly, elevated concentrations are also evident in comparison to average concentrations of Zn (67 µg/g, between 2 and 395 µg/g), Co (145 µg/g, between 15 and 640 µg/g), and Ni (977 µg/g, between 105 and 2160 µg/g) in Paleoproterozoic pyrite from other localities (Large et al., 2014). *In situ* analyses of pyritized fossilized structures show even higher Zn, Co, and Ni concentrations of up to 1445, 2900, and 4156 µg/g, respectively, compared to diagenetic pyrite concretions unrelated to fossilized structures with Zn < 50 µg/g, Co < 200 µg/g, and Ni < 700 µg/g (Fig. 4, Table S1). Manganese and Ag concentrations in fossilized forms, up to 1143 and 36 µg/g, respectively, are also higher than those in diagenetic pyrite concretions unrelated to fossilized structures (214 and 3 µg/g, respectively; Fig. 4, Table S1).

The δ^{66}Zn values of the Francevillian Group shales and marine carbonates range between 0.227 and 0.959‰, with a mean of 0.413‰ (Fig. 1; Table S2), which is generally slightly higher than the average detrital input value of ~0.33‰ (Little et al.,

2014). Microbial mat structures, diagenetic pyrite concretions unrelated to fossilized structures, thin early diagenetic pyrite beds, and diagenetic carbonate concretions of the Francevillian Group have similar δ^{66}Zn values to host rocks, shale and marine carbonate (Fig. 5; Table S2). Correction to authigenic composition by subtracting the estimated detrital contribution (Little et al., 2016) yields only marginally higher δ^{66}Zn values (Fig. 1; Table S2). By contrast, the Zn isotopic composition (δ^{66}Zn) of pyritized and non-pyritized fossilized structures ranges between –0.152 and 0.162‰, which is isotopically lighter than that of the host sediments, microbial mat structures, and early diagenetic pyrite beds and concretions, with an offset (δ^{66}Zn of fossilized structures - δ^{66}Zn of host sediments) between –0.221 and –0.526‰ with respect to bulk sediment values (which is only slightly increased for estimated authigenic values; Table S2, Figs. 2 and 5). The δ^{66}Zn values tend to be more negative for the larger specimens, regardless of the degree of pyritization, resulting in a negative correlation between Zn concentrations and δ^{66}Zn values in fossilized structures (Figs. 2, 5A, 5B). Archean, Phanerozoic, and modern diagenetic pyrite concretions unrelated to fossils are isotopically unfractionated from their host sedimentary rocks (Table S2).
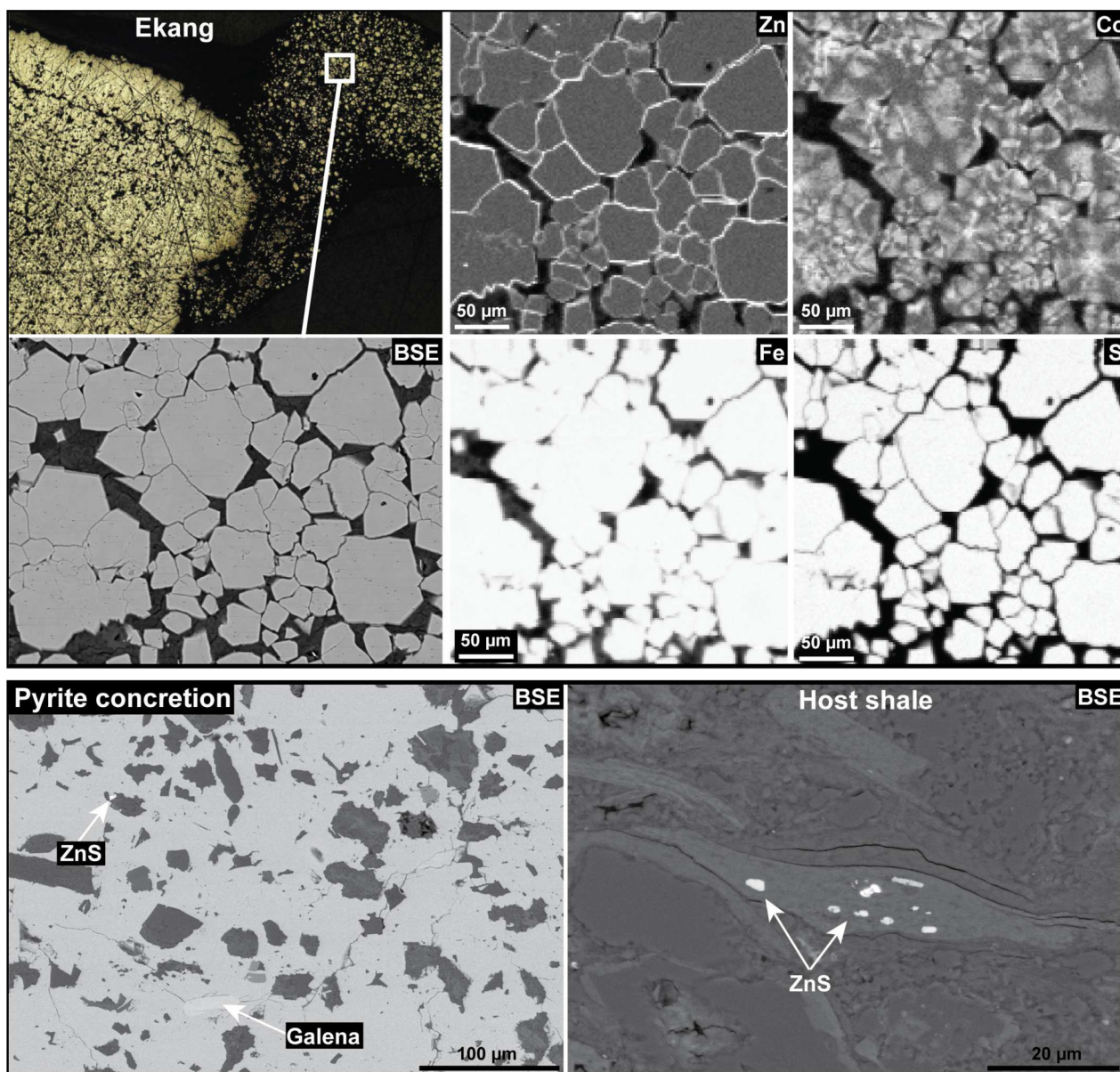
Fig. 3. The upper panel of the figure shows reflected light and backscattered electron (BSE) images of the specimen Ekang and related electron microprobe elemental maps of Zn, S, Fe, and Co. The white empty square on the reflected light microscope image shows the area from which the data (BSE and elemental maps) are derived. In BSE image, grey sub-rounded to subhedral pyrite (FeS$_2$) grains are surrounded by thin, light-grey rims that are Zn-enriched. These thin rims are depleted in S (thin grey margins), but not in Fe, which indicates that the Zn enrichment is not linked to pyrite or sphalerite ((Zn,Fe)S). The texture of these rims (e.g., preservation between grain contacts) shows that they were already in place before the growth of pyrite. Distribution of Co is controlled by the growth of pyrite and does not show a similar pattern to Zn, which further supports the notion that distribution of Zn in the fossilized structures is not determined by pyritization. The lower panel of the figure shows BSE images of a diagenetic pyrite concretion not associated with fossilized structures and host shale. The concretion is characterized by homogeneous pyrite and shows no internal Zn organization, but contains inclusions of galena (PbS) and sphalerite. The host shale also shows disseminated sphalerite. Both fossilized structure and concretion are from the same host black shale.
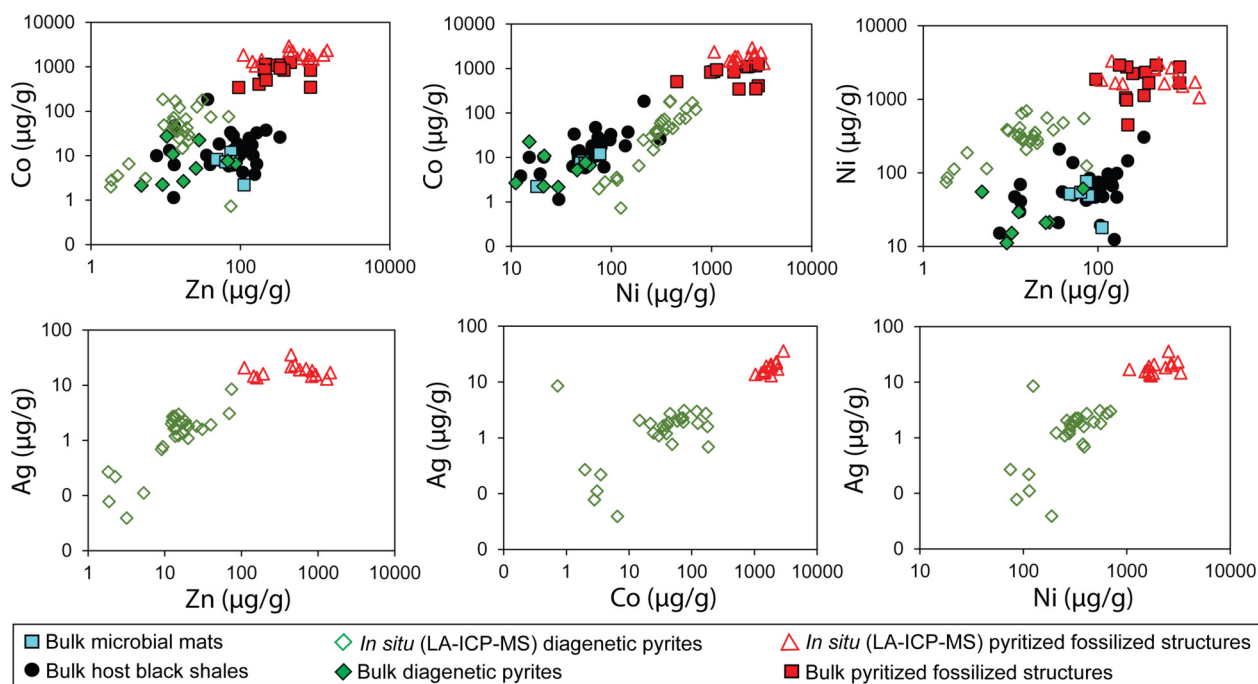
4. Discussion

4.1. Origin of Zn enrichments and low $\delta^{66}Zn$ values in the Francevillian Group fossilized structures

Zinc concentrations in the Francevillian Group fossilized structures are at least one order of magnitude higher than in their host rocks and other materials studied here. These fossilized structure-related Zn fractions are also characterized by significantly lower $\delta^{66}Zn$ values with respect to those of the respective host rocks and microbial mat structures. Several processes in the marine realm can cause Zn enrichment and its isotopic fractionation, including hydrothermal processes, precipitation of a zinc sulfide (ZnS) phase,

non-quantitative incorporation of Zn into pyrite, Zn chelation by organic or inorganic compounds, fast pyrite crystal growth, and biological uptake (Fujii et al., 2011; John et al., 2007, 2008; Köberich and Vance, 2019; Vance et al., 2016; Viers et al., 2007; Weiss et al., 2005; Wilkinson et al., 2005; Zhang et al., 2019). A detailed assessment of these processes is thus required to evaluate the origin of Zn enrichments and low $\delta^{66}Zn$ values in the Francevillian Group fossilized structures, thus helping to resolve whether the geochemical and isotopic signatures reflect primary Zn uptake by the Paleoproterozoic biota, or abiotic Zn processing in seawater or during diagenesis.

Hydrothermal processes, both submarine during sediment deposition and via late circulating fluids after deposition, are po-

Fig. 4. Bulk and *in situ* analyses showing variations in trace metal concentrations of the Francevillian Group fossilized structures, microbial mat structures, fossilized structure-unrelated pyrites, and host rocks.

tential sources for light Zn isotope composition and may explain the Zn geochemical signature found in the Francevillian Group fossilized structures (e.g., John et al., 2008; Wilkinson et al., 2005; Zhang et al., 2019). However, converging observations provide strong evidence against a hydrothermal origin for the light Zn isotopic composition of the fossilized structures. These include the highly negative $\delta^{34}S$ values of the pyritized, fossilized structures along with diagenetic pyrite concretions unrelated to fossilized structures and their host rocks, as low as −30‰, which are typical for microbial sulfate reduction in the sediments and/or at the water-sediment interface during early diagenesis (El Albani et al., 2010, 2014; Ossa Ossa et al., 2013, 2018). Pre-compaction pyritization in these black shales is also indicated by the imprints left by the fossilized structures in the host rocks (Fig. 2). Furthermore, sediment laminae wrapping around both the fossilized structures and diagenetic pyrite concretions unrelated to fossilized structures (e.g., specimen Aki in Figs. S1, S4D, and S4E), are consistent with their pre-compaction and pre-lithification origin. It also seems unlikely that submarine hydrothermal activity would selectively affect both pyritized and non-pyritized Francevillian Group fossilized structures, but not their host lithologies or laterally and stratigraphically adjacent microbial mat structures and fossil-unrelated early diagenetic pyrite concretions. Furthermore, hydrothermal processes related to late circulating fluids can be ruled out by the preservation of abundant mixed layer illite/smectite clay minerals, together with a dominant illite phase with a 1Md polytype clay component (El Albani et al., 2010; Ossa Ossa et al., 2013). This indicates a diagenetic clay mineral transformation – smectite to illite conversion – through a solid-state transformation in a closed system that was not affected by late-stage fluid-rock interaction and/or high-temperature hydrothermal processes (Ossa Ossa et al., 2013 and references therein). In view of these observations, it appears unlikely that Zn and other trace-metal enrichments, together with lower $\delta^{66}Zn$ values found in the Francevillian Group fossilized structures, are linked to hydrothermal processes. They rather reflect pristine geochemical signatures of the primary structures that were fossilized in the Francevillian Group marine sediments.

It has been demonstrated that precipitation of ZnS or non-quantitative incorporation of Zn into pyrite can result in an enrichment in light Zn isotopes in the precipitating phase (Fujii et al., 2011; Vance et al., 2016). A proposed conceptual model for the formation of pyrite-zinc sulfide framboids within organic-rich sediment suggests that late ZnS rims precipitate around microbially induced pyrite crystals during diagenesis (Hu et al., 2018). This might potentially explain our observations regarding Zn distribution and isotopically light signals in the pyritized Francevillian Group fossilized structures. While Zn-enriched zones were observed in EPMA elemental maps, these zones are not marked by lower Fe concentrations as would be expected for ZnS phases (Fig. 3). Furthermore, *in situ* elemental analyses using EPMA and LA-ICP-MS gave nearly constant Fe/S ratios of ∼0.9 (Table S1), which is characteristic of pyrite rather than sphalerite and argues against ZnS precipitation in association with fossilized structures. Disseminated sphalerite and galena inclusions were observed within fossil-unrelated diagenetic pyrite concretions and host shale (Fig. 3), but these yield lower Zn concentrations and higher $\delta^{66}Zn$ values relative to pyritized fossilized structures from the same stratigraphic level. Precipitation of ZnS can thus be ruled out as a potential explanation for the enrichment in light Zn isotopes in the fossilized structures. By the same token, the possibility for late ZnS overgrowth on microbially-induced pyrite crystals during diagenesis (Hu et al., 2018) can also be ruled as an explanation for the ∼10-100 μm-sized subrounded and subhedral pyrite grains with thin Zn-enriched rims revealed by Zn EPMA maps of fossilized structures (Fig. 3). Microtextural evidence (i.e., preservation of the continuous net of rims at the contact of pyrite crystals) clearly indicates that the framework represented by these Zn-enriched rims was already in place before the growth of pyrite and was deformed by their growth (Fig. 3). Therefore, pyritization seems to have occurred within an organic framework already enriched in Zn.

Fast growth of pyrite crystals in organic matter-rich sediments might promote metal enrichments and kinetic Zn isotope fractionation and thus provides a further possible explanation for higher Zn concentrations and lower $\delta^{66}Zn$ values found in the Francevillian Group fossilized structures. The same applies to non-quantitative
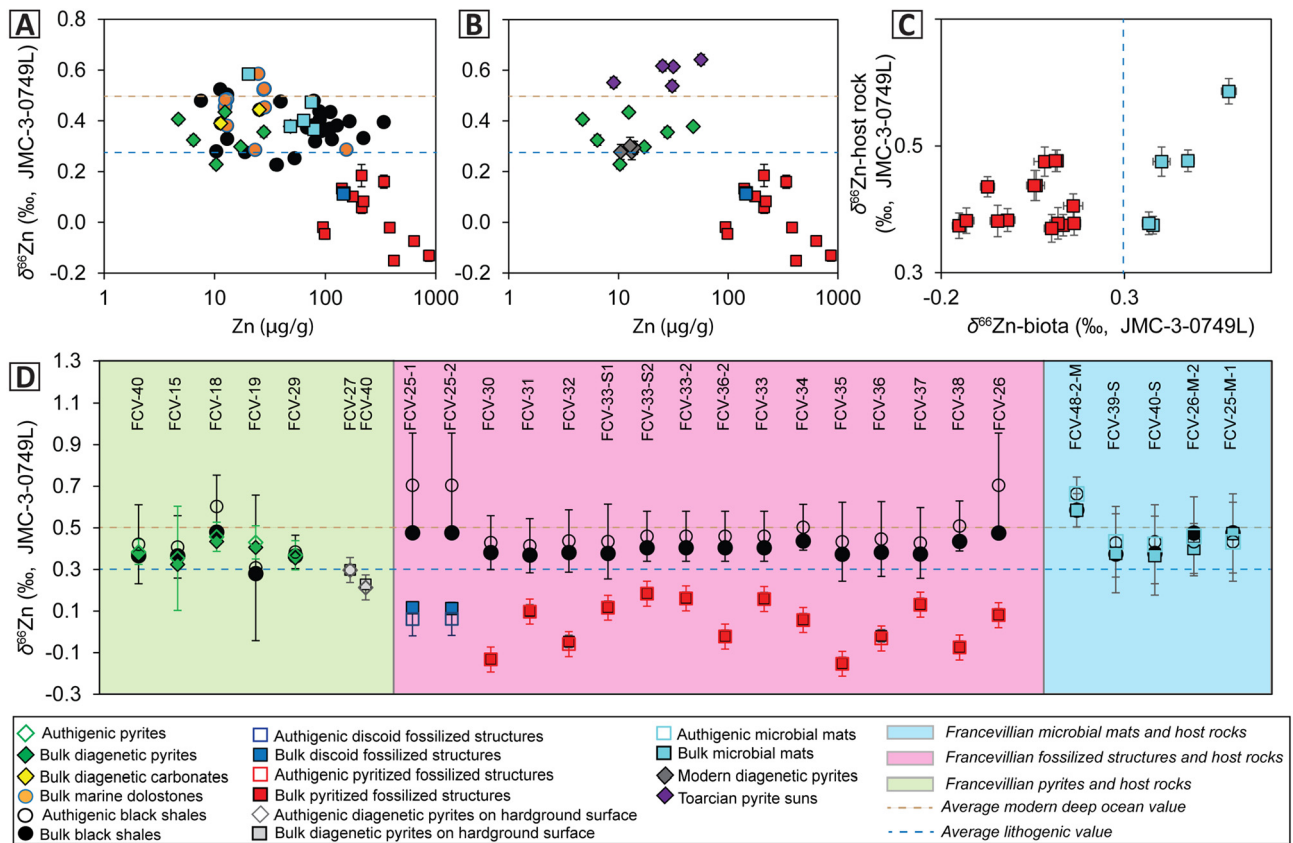
Fig. 5. Cross-plots of Zn concentration vs. δ^{66}Zn isotopic composition for (**A**) pyritized Francevillian fossilized structures, microbial mats structures, and their respective host sediments, and (**B**) diagenetic pyrite of various ages (Figs. 2, S1, S4, S5), including Paleoproterozoic (Francevillian Group, Gabon), Phanerozoic (lower Toarcian, Germany), and modern (Richards Bay, South Africa). Pyritized Francevillian fossilized structures have much higher Zn concentrations and lower δ^{66}Zn values compared to both their host sediments and diagenetic pyrite unrelated to fossilized structures. (**C**) Cross-plots of δ^{66}Zn values of pyritized Francevillian fossilized structures and microbial mat structures (δ^{66}Zn-biota) vs. δ^{66}Zn values of their respective host rocks (δ^{66}Zn-host rock). (**D**) Bulk and authigenic Zn isotopic composition of the Francevillian basin fossilized structures, microbial mat structures, and their respective host sediments. Data for the pyritized Francevillian basin fossilized structures is consistent with biological uptake of isotopically light Zn by eukaryotic organisms in a marine environment c. 2.1 Gyrs ago. Panels (**A**) and (**B**) show a negative correlation between Zn concentrations and δ^{66}Zn values, mostly for fossilized structures, which is mainly controlled by the size of the fossilized structures (see Figs. 2, S1). Error bars on δ^{66}Zn values represent individual analysis 2SE and 2SD obtained during measurements (bulk) and for an estimate of authigenic composition (authigenic), respectively (see Table S2).

incorporation of Zn into pyrite. However, not all of the Francevillian Group fossilized structures studied here are pyritized. The discoid, poorly to unpyritized Engong specimens (Fig. 2) also show lighter Zn isotopic composition than their host black shales, similar to the pyritized structures. As argued above, where fossilized structures are pyritized, fast growth of pyrite crystals and/or non-quantitative incorporation of Zn into pyrite are unlikely explanations since they cannot explain why other fossil-unrelated pyrite concretions, occurring laterally within a few centimeters from fossilized structures in the same sedimentary beds, do not record trace-metal enrichments and lower δ^{66}Zn values relative to the host rocks. Furthermore, the Toarcian pyrite suns from the Posidonia Schist of the Swabian Alb in SW Germany, which indeed formed by rapid pyritization in black shales (Seilacher, 2001), offer an excellent analogue to test the effect of fast pyrite growth on Zn geochemical behavior in organic-rich sediments. The data do not show unusually high trace-metal enrichments in pyrite suns and their δ^{66}Zn values overlap with those of their host black shales, arguing against a significant control of fast pyrite growth over trace-metal enrichment and Zn isotope fractionation. Therefore, higher Zn concentrations and lower δ^{66}Zn values found in pyritized and unpyritized Francevillian Group fossilized structures relative to their host rocks and microbial mat structures strongly suggest that the Zn signal recorded by these Paleoproterozoic fossilized structures is not linked to the precipitation of sulfide phases.

Organisms can mediate metal isotope fractionation through preferential uptake during transport across the cell membrane, yielding an enrichment in light Zn isotopes (John et al., 2007; Samanta et al., 2018). This metabolic Zn handling is the most likely process to explain the high Zn concentrations and low δ^{66}Zn values of the Francevillian Group fossilized structures. The line of evidence provided above thus suggests that both unpyritized and pyritized Francevillian Group fossilized structures are likely fossils. Therefore, their Zn geochemical signature, mainly controlled by the way these life forms handled Zn, can help to further elucidate the nature and origin of the organisms involved.

As a bio-essential micronutrient, Zn is a component in several metalloenzymes that serve in key biological functions in both eukaryotic and prokaryotic cells (Andreini et al., 2006; Costello and Franklin, 1998; Dupont et al., 2010; Eide, 2003, 2006; John et al., 2007; Outten and O'Halloran, 2001; Samanta et al., 2018; Vallee and Falchuk, 1993; Viers et al., 2007; Weiss et al., 2005). Cellular Zn demand strongly depends on cell size, organizational complexity, functionalities, and metabolism, whereas Zn uptake and its trafficking through the plasma membrane, as well as its intracellular distribution, are driven by several families of transporter proteins (Andreini et al., 2006; Costello and Franklin, 1998; Dupont et al., 2010; Eide, 2003, 2006; John et al., 2007; Outten and O'Halloran, 2001). The cellular trafficking of Zn is controlled by a regulatory mechanism (known as Zn homeostasis), which is determined by the total Zn quota required for optimal

cell growth (Eide, 2003; Outten and O´Halloran, 2001; Vallee and Falchuk, 1993). The exact mechanisms by which Zn is transported through the cell and organelle membrane remain unclear. However, the current view is that transporter proteins use the gradient of other ions (e.g., HCO_3^{--} for uptake and H^+ or K^+ for efflux), to facilitate diffusion of Zn through cytoplasmic loops spanning the membrane (Eide, 2006). Transmembrane loops may also bind Zn during this transport and favor its accumulation in the plasma membrane (Costello and Franklin, 1998; Eide, 2006). Importantly, the Francevillian Group fossilized structures have been previously interpreted as colonial multicellular organisms with a likely "slime mold" style of coordinated behavior and motility (El Albani et al., 2010, 2019). Considering that cellular Zn homeostasis is driven by transporter protein influxes and effluxes through transmembrane loops across cell walls (Eide, 2003, 2006; John et al., 2007), we interpret the observed rimmed pyrite grains of the pyritized Francevillian Group fossilized structures to represent replacement of ancient cells of Paleoproterozoic living organisms, with the thin Zn-enriched rims of the pyrite grains being fossilized cell walls. Zinc was likely accumulated within the plasma membrane for either protecting cells against toxicity related to high extracellular Zn concentrations, or to ensure Zn availability for intracellular processes under low external Zn conditions. Regardless of the exact cause for such cell wall Zn accumulation, it appears that the Francevillian Group fossilized structures are remnants of preserved Paleoproterozoic biota, which had already acquired a complex Zn regulatory system.

Alternatively, micro-organisms can also enrich Zn as adsorbed extracellular coatings. This is different from the intracellular Zn inventory, which is mainly acquired through biological uptake. This kind of extracellular Zn enrichment might be the case for the cyanobacterium *Synechococcus* sp. CCMP 2370 (Köbberich and Vance, 2019). In this case, high Zn enrichment would reflect Zn adsorption, which is potentially driven by iron oxides coating cyanobacteria, rather than by biological uptake (cf. Köbberich and Vance, 2019). Furthermore, *Synechococcus* sp. CCMP 2370 yielded heavy Zn isotopic composition indistinguishable from that of the initial media (Köbberich and Vance, 2019), which is more consistent with adsorption rather than biological uptake. Extracellular Zn enrichment on micro-organisms and/or as coatings on pyrite grains has also been suggested for sulfate-reducing bacteria (Hu et al., 2018). For the Francevillian Group fossilized structures, *in situ* elemental analysis using EPMA and LA-ICP-MS revealed pyrite grains within the fossilized network with Zn concentrations of up to 1445 ppm (for variation in Zn concentration *versus* molar Fe/S ratios see Table S1) and without Zn-rich rims on pyrite grains and/or fossilized bodies. This indicates that the high Zn enrichments did not result from Zn coatings on cells or pyrite grains, but rather, Zn likely accumulated within intracellular mass and cell membrane through biological uptake. Therefore, Zn homeostasis was indeed a biological process that these Paleoproterozoic organisms used in order to maintain their intracellular Zn quota for achieving a better gene expression for their potentially complex metabolism, growth, and reproduction.

4.2. Eukaryotic vs. prokaryotic level of Zn enrichment and preferential uptake of light Zn isotopes by the Francevillian Group biota

As discussed above, the enrichment in light Zn isotopes observed in the Francevillian Group fossilized structures appears to represent a primary signature related to the life cycle of Paleoproterozoic organisms. The level of Zn enrichment and associated isotopic fractionation in the Francevillian Group fossilized structures, relative to the authigenic signature in host rocks, may help to resolve their prokaryotic vs. eukaryotic affinity. In prokaryotic cells, Zn homeostasis is largely dominated by uptake and efflux

transporters (Brocklehurst et al., 1999; Patzer and Hantke, 1998), whereas the storage of excess intracellular Zn is extremely limited (Outten and O´Halloran, 2001). By contrast, three main families of Zn transporters drive intracellular Zn homeostasis in eukaryotic cells, including those involved in the uptake, efflux, and sequestration into cellular sites, such as the vacuole (Eide, 2003), indicating that large intracellular Zn excess can be accumulated and stored within eukaryotic cellular compartments (Nasir et al., 1999; Ramsay and Gadd, 1997). Although both prokaryotic and eukaryotic cells can concentrate Zn, the eukaryotic Zn demand, uptake rate, and sequestration capability are much higher relative to those for prokaryotes, while molecular and phylogenomic analyses show that Zn-binding proteins are more abundant in eukaryotes relative to bacteria and archaea (Andreini et al., 2006; Dupont et al., 2010). Therefore, a higher eukaryotic Zn inventory differs from bacterial and archaeal enzyme requirements due to the higher complexity of the cell structure, a more sophisticated metabolism, and more complex physiological processes (Andreini et al., 2006; Costello and Franklin, 1998; Dupont et al., 2010; Eide, 2003, 2006; Nasir et al., 1999; Ramsay and Gadd, 1997). The higher level of Zn enrichment found in the Francevillian Group fossilized structures compared to microbial mat structures and host rocks may thus reflect a typical eukaryotic high uptake rate due to more complex and diverse Zn handling by organisms of this biota.

However, the possibility to differentiate eukaryotic and prokaryotic cells based on their Zn uptake rate and associated preferential enrichment in light Zn isotopes has recently been challenged (Köbberich and Vance, 2019). According to this study, some eukaryotes can yield similar Zn uptake rates (corresponding to cellular Zn demand), and Zn/C and Zn/P ratios, as well as $\delta^{66}Zn$ values, to prokaryotic phytoplankton, indicating that caution should be exercised when comparing these two clades using their Zn signals. However, in this experimental work, the diatom *Chaetoceros* sp., a eukaryote shown to yield similar Zn uptake rates to those of prokaryotes (cyanobacteria), was cultured on urea. By contrast, when grown on nitrate, Zn uptake rates for this eukaryote were more than 5 times higher than those of any cyanobacteria (Köbberich and Vance, 2019). Nitrate and urea are known to be a source of nitrogen for growth and biomass production in phytoplankton. Importantly, it has been shown that urea can have a repressive effect on the growth and metabolism of *Chaetoceros* sp. (Arzul et al., 1996). Since the amount of produced biomass by *Chaetoceros* sp. in these growth experiments (Köbberich and Vance, 2019) was neither determined nor estimated, it is difficult to evaluate the effect of urea on the diatoms metabolism and Zn uptake rate. Consequently, a low metal uptake rate (similar to that of cyanobacteria) shown by the diatom *Chaetoceros* sp. growing on urea (Köbberich and Vance, 2019) might be induced by imposed experimental conditions, rather than an intrinsic eukaryote characteristic.

Moreover, for both prokaryotic and eukaryotic phytoplanktonic photosynthetic organisms, a significant part of intracellular Zn is used in metalloenzymes that facilitate carbon fixation (e.g., via carbonic anhydrase) and phosphorus acquisition (e.g., via alkaline phosphatase) (Morel et al., 1994; Shaked et al., 2006). It can thus be conceived that phytoplanktonic photosynthetic prokaryotes and eukaryotes would yield indistinguishable Zn/C and Zn/P ratios when their Zn requirement for intracellular Zn inventory is only to sustain C and P acquisition. However, there is also a wide range of complex Zn-dependent functionalities in eukaryotic cells, not found in prokaryotes, that have been shown to require high amounts of Zn. This is the case for the vacuole and other vesicular components of eukaryotic cells, not found in prokaryotes, that can take up, store and maintain high levels of intracellular Zn (Eide, 2003; Nasir et al., 1999; Ramsay and Gadd, 1997). The same applies to some intracellular organelles, such as mitochondria, which

require large amounts of Zn to generate chemical energy to power the cell (Costello et al., 2004). Therefore, comparing the cellular Zn inventory between eukaryotes and prokaryotes, based only on their estimated Zn/C and Zn/P ratios (Köbberich and Vance, 2019), when other, complex eukaryotic Zn-dependent functionalities are not expressed, considerably underestimates the capacity for eukaryotic cells to store and develop higher levels of Zn than prokaryotes.

In growth experiments (Köbberich and Vance, 2019), the bioavailable Zn pool was significantly depleted and isotopically fractionated by a strong organic ligand before it interacted with organisms. Organic ligands preferentially bind isotopically heavy, dissolved Zn, resulting in a small bioavailable Zn pool enriched in light isotopes (Köbberich and Vance, 2019). Both prokaryotes and eukaryotes growing in this small bioavailable Zn pool will preferentially take up light Zn isotopes through high-affinity transport, yielding indistinguishable δ^{66}Zn values (Köbberich and Vance, 2019). Furthermore, a high level of intracellular Zn enrichment in prokaryotes, relative to the environmentally bioavailable Zn concentrations, can only develop under Zn-starved conditions (Outten and O'Halloran, 2001). This has been shown for the bacterium *Escherichia coli*, which can yield an intracellular Zn content several orders of magnitude higher than that of the extracellular dissolved Zn pool, reaching millimolar levels in total intracellular Zn (Outten and O'Halloran, 2001). By contrast, under Zn-replete conditions, prokaryotic cells are likely to use low-affinity uptake and yield intracellular Zn concentrations close to the ambient bioavailable Zn content (Outten and O'Halloran, 2001). Importantly, high levels of intracellular Zn are usually toxic and even lethal for most prokaryotes (Perez and Chu, 2020). For example, experimental work demonstrated that a Zn concentration of 50 mg/L is lethal to cyanobacterium *Synechococcus* sp. (Perez and Chu, 2020). Eukaryotic cells acquire Zn at concentrations several times higher than in the bioavailable Zn pool (regardless of its size) (John et al., 2007), since they have more complex physiological functionalities, not found in prokaryotes, through which they can develop and store high levels of intracellular Zn (Costello and Franklin, 1998; Costello et al., 2004; Eide, 2003; Eisler, 2009; Nasir et al., 1999; Ramsay and Gadd, 1997). Therefore, if an organism develops Zn concentrations several times higher than that of the environment under Zn-unlimited conditions, that organism is likely to have an affinity to eukaryotes since their complex physiologies and metabolisms depend on readily available intracellular Zn.

It would be difficult to differentiate eukaryotes and prokaryotes if the Francevillian basin marine habitats were starved in Zn and enriched in light Zn isotopes, because under these conditions both clades would yield indistinguishable Zn signals (Köbberich and Vance, 2019; Outten and O'Halloran, 2001). However, bulk and *in situ* analyses of the Francevillian Group host black shales and matrix show authigenic Zn enrichments (up to 126 µg/g) relative to average upper continental crust (67 µg/g) (see Fig. 1B; Table S2). This indicates that the Francevillian basin marine habitats did not experience Zn starvation. Prokaryotes growing in Zn-replete marine habitats would not enrich Zn in their intracellular pool beyond the order of Zn concentrations in the bioavailable Zn pool (cf. Outten and O'Halloran, 2001). This is consistent with the Francevillian Group microbial mats (produced by prokaryotes) yielding indistinguishable or even lower Zn concentrations with respect to those of the host rocks or matrix (Table S2; Figs. 4 and 5). By contrast, levels of Zn enrichment (up to 1445 µg/g) found in the Francevillian Group fossilized structures are up to 16 times higher (Tables S1, S2; Figs. 4 and 5). Because prokaryotes would not develop such Zn enrichments in a Zn-unlimited pool, high levels of Zn enrichment found in the Francevillian Group fossilized structures, compared to host rocks and microbial mat structures, are best explained by eukaryotic Zn uptake under Zn-unlimited conditions.

Furthermore, although the above discussed experiments (Köbberich and Vance, 2019) demonstrate that both eukaryotes and prokaryotes can yield low δ^{66}Zn values when grown in an isotopically light Zn pool, there is no evidence from either natural environments or experiments to argue that prokaryotes could significantly fractionate Zn isotopes during uptake, whereas this process has been observed for a wide range of photosynthetic eukaryotes (John et al., 2007; Samanta et al., 2018; Viers et al., 2007; Weiss et al., 2005). In the Francevillian basin, the authigenic Zn isotope composition of the host rocks, as well as the Zn isotope composition of early diagenetic pyrite beds, marine carbonates, early diagenetic pyrite (not associated with fossilized structures), and carbonate concretions, clearly demonstrates that Zn was bioavailable in both sediment pore-water and the overlying water column and was enriched in heavy Zn isotopes at the time it interacted with organisms (see Supplementary Text for further discussion). For the case of organic ligands preferentially binding isotopically heavy Zn, both fossilized structures and microbial mat structures should be isotopically light. This is not the case here since the δ^{66}Zn values of the microbial mat structures are most consistent with their prokaryotic origin (range between 0.366 and 0.585‰), as they are isotopically indistinguishable from host shales and carbonates (range between 0.378 and 0.586‰; Fig. 5; Table S2). Although Zn metalloenzymes can be expressed in bacteria, their utilization by these mid-Paleoproterozoic microbial mats was not associated with obvious Zn isotopic fractionation and cannot explain the low δ^{66}Zn values observed in the Francevillian Group fossilized structures. These observations together suggest that the low δ^{66}Zn values observed for the Francevillian Group fossilized structures relative to the isotope composition of the bioavailable Zn pool in their environment is also best explained by isotopic fractionation during eukaryotic uptake. However, it is important to emphasize here that studies of Zn isotope fractionation by eukaryotes have been focused exclusively on modern photosynthetic eukaryotes. This leaves the uncertainty whether strong enrichment in light Zn isotopes represents a distinct trait of the whole eukaryotic domain and whether the Francevillian Group fossilized structures represent photosynthetic or non-photosynthetic eukaryotes.

4.3. Further elemental evidence for eukaryotic affinity

Bulk analyses of the Francevillian Group host rocks, diagenetic pyrite concretions, pyrite beds, and diagenetic carbonate concretions show authigenic enrichments in Co and Ni relative to the crustal average. This suggests that the Francevillian basin marine habitats were also characterized by unlimited conditions in terms of these metals, as has previously been shown for Mn (Gauthier-Lafaye and Weber, 2003; Ossa Ossa et al., 2018). However, bulk and *in situ* analyses show that the Francevillian Group fossilized structures are characterized by even higher levels of Co, Ni, Mn, and Ag enrichment relative to the other materials investigated (Fig. 4; Tables S1-S3). Metal enrichments found in both the pyritized and non-pyritized fossilized structures studied here provide strong evidence for primary signatures related to the Francevillian biota, rather than the pyritization process in seawater or during diagenesis. The uptake of these metals by eukaryotes and prokaryotes, which is mainly driven by differences in complexity and physiological functionalities between the two clades, can help to shed further light on the biological affinity of the Francevillian biota. For example, cyanobacteria need Co to synthesize cobalamin cofactors, but when limited by Co, the growth rate of *Prochlorococcus* MIT 9215 has been shown to drastically decrease at high Zn and Mn levels, compared to their low levels, indicating that Zn and Mn are competing for the same transporters with Co (Hawco and Saito, 2018). This competitive inhibition shows that Co, Zn, and Mn are unlikely to be enriched together by the same cyanobacteria in the

Francevillian basin marine habitats. This, however, contrasts with eukaryotic cells, which co-enrich Co and Zn through their various complex physiological functionalities (Hawco and Saito, 2018). Furthermore, the cyanobacterium *Synechococcus* only utilizes high-efficiency uptake to yield intracellular levels of Ni and Co required for synthesis of Ni(II) and Co(II) enzymes and coenzyme B_{12} for its growth if it is exposed to starved environmental conditions with respect to these metals (Huertas et al., 2014). This means that Ni and Co unlimited habitats, like in the Francevillian basin, would not induce high levels of Ni and Co enrichment in cyanobacteria. Consequently, it is unlikely that cyanobacteria in the Francevillian basin would yield high Mn, Co, Ni, and Zn enrichments, which is indeed supported by lower concentrations in the Francevillian Group microbial mats compared to fossilized structures. By contrast, due to the complexity of eukaryotic cells, intracellular organelles, specific to eukaryotes, such as the vacuole, may act as efficient detoxifiers to remediate and store intra- or extracellular metal excess. This could ultimately co-enrich eukaryotic cells in these metals and explain the high Co, Ni, Zn, and Mn concentrations found in the Francevillian Group fossilized structures, which further points to their possible eukaryotic affinity.

Although Ag analyses were not made on bulk host rocks and microbial mat structures, LA-ICP-MS data show that Ag is enriched in the Francevillian Group fossilized structures, with concentrations ≥ 10 μg/g, compared to early diagenetic pyrite unrelated to these structures, with concentrations < 10 μg/g (Fig. 4; Table S1). The same applies to other Paleoproterozoic pyrite with Ag concentrations averaging 3 μg/g (ranges between 1 and 7 μg/g; Large et al., 2014). Considering that diagenetic pyrite is an authigenic mineral phase prone to record environmental geochemical conditions, Ag concentrations found in these pyrite phases likely reflect the aqueous Ag concentration in seawater (for pyrite beds) and sediment pore-waters (for concretions). Therefore, higher Ag concentrations in pyritized fossilized structures relative to diagenetic pyrite unrelated to these structures suggest that organisms of the Francevillian biota were able to enrich Ag from their depositional environment. Silver uptake is well known for eukaryotes (Eisler, 2009; Malysheva et al., 2021; Qian et al., 2016; Wang et al., 2016), which is not the case for prokaryotes (Atiyeh et al., 2007; Boxall et al., 2007; Dedman et al., 2020; Duong et al., 2016). At certain levels, Ag can be toxic (causing respiratory and growth disturbance) for both eukaryotic and prokaryotic organisms (Dedman et al., 2020; Duong et al., 2016; Kadukova, 2016; Malysheva et al., 2021; Qian et al., 2016; Wang et al., 2016). However, Ag concentrations in sediments on the order of magnitude yielded by the Francevillian Group fossilized structures are commonly found not to be toxic to eukaryotic cells (Eisler, 2009; Malysheva et al., 2021; Qian et al., 2016; Wang et al., 2016). Such eukaryotic cellular Ag concentrations result from uptake of dissolved Ag or Ag released from Ag nanoparticles (AgNPs), coupled with intracellular bio-transformation to sulfidized (e.g., β-Ag_2S and Ag-thiolates) or non-crystalline phases that can be stored in cellular compartments (Malysheva et al., 2021; Wang et al., 2016). The *Chlorella vulgaris* green algae can adapt to high Ag levels by detoxifying Ag via induction of antioxidant enzymes (Wang et al., 2016). The same applies to other algae such as *Parachlorella Kassleri* (Kadukova, 2016). By contrast, Ag is highly toxic to bacteria (Atiyeh et al., 2007) and AgNPs have been extensively used in modern industry for their strong antibacterial properties (Boxall et al., 2007). For example, an Ag concentration of ≥ 10 μg/g has been shown to be highly toxic for cyanobacterium *Prochlorococcus* (Dedman et al., 2020) and at 1 μg/g for cyanobacterium *Microcystis aeruginosa* (Duong et al., 2016), whereas green algae thrive under such intracellular Ag concentrations (Qian et al., 2016). A wide range of eukaryotes can perform intracellular biotransformation of Ag and store it in cellular compartments to protect against Ag toxicity,

which is unlikely to be the case for bacteria or prokaryotes. Therefore, Ag enrichments found in the Francevillian Group fossilized structures provide another line of evidence in support of their eukaryotic affinity.

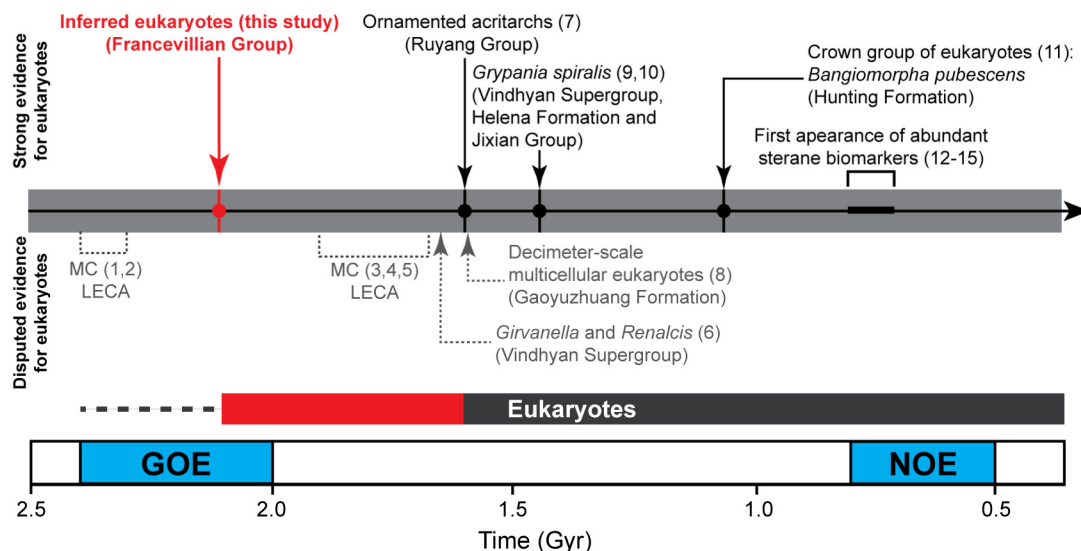### 4.4. The Francevillian Group organisms: evolutionary response to the GOE?

Based on the high Zn, Co, Ni, and Mn demand of eukaryotes and preferential uptake of light Zn isotopes, our dataset provides compelling geochemical evidence to suggest both a biogenic and eukaryotic affinity for the c. 2.1 Gyr old Francevillian Group fossilized structures. If correct, this would suggest that eukaryotes already evolved during the latter part of the GOE. This is consistent with earlier suggestions based on molecular clocks (Gold et al., 2017; Strassert et al., 2021) that eukaryotes evolved at least 400 Myr earlier than indicated by paleontological and biomarker records (Fig. 6). Our findings suggest that complex life forms might have rapidly adapted to the appearance of atmospheric oxygen with the emergence of oxygen-dependent and energetically more efficient eukaryotic metabolism, thus adding to the growing evidence that environmental change, specifically oxygenation of Earth's surface environments, was a major driver of biological evolution.

5. Summary and conclusions

The high concentrations of Zn and associated negative Zn isotope fractionations recorded by the Francevillian Group fossilized structures, are an important, inorganic biogeochemical marker for the biogenicity and potential affinity of these structures. Enrichment in light Zn isotopes in fossilized structures, relative to their host rocks, potentially provide a new proxy to track the emergence and evolution of eukaryotes in deep time, especially when traditional morphological and organic geochemical tools do not allow unequivocal identification of biological affinity. However, the use of this inorganic, geochemical biomarker is not straightforward for tracking early evolution of life. First, it is critical to thoroughly assess whether abiotic processes such as hydrothermal activity and chelation by inorganic or organic ligands could explain Zn enrichments and associated negative Zn isotope fractionations in fossilized structures. Second, it is critical to constrain the geochemical composition of the bioavailable Zn pool at the time when it interacted with organisms in their habitats. Finally, fossilized structures have to be Zn-enriched and negatively isotopically fractionated relative to their host rocks. It is therefore important to first address the three points highlighted above before a meaningful interpretation of biological affinity of fossilized structures is attempted.

Enrichment in light Zn isotopes in fossilized structures could reflect hydrothermal processes and high-affinity biological uptake if the host rock is also characterized by light Zn isotope compositions. This is because hydrothermal fluids are a potential source for light Zn isotopes, which would equally affect the host rocks and fossilized structures. Furthermore, in the case of high-affinity biological uptake, it is almost impossible to differentiate prokaryotes from eukaryotes using their Zn geochemical signatures if they grew under low Zn and/or heavy Zn isotope-depleted environmental conditions because they would similarly uptake from this Zn pool with no fundamental difference in their Zn concentrations and isotopic compositions. Another ambiguous scenario is when fossilized structures are enriched in heavy Zn isotopes relative to their host rocks. In both of the latter cases, it would be impossible to differentiate the effect of Zn chelation/adsorption (by organic or inorganic molecules) from biological uptake, as well as prokaryotic vs. eukaryotic Zn handling.

Finally, in a scenario where fossilized structures are enriched in Zn with light isotopic composition relative to their host rocks,

Fig. 6. Timeline for the Proterozoic eukaryote record showing an inferred early evolution of eukaryotes by the latter part of the GOE at c. 2.1 Gyrs based on this study of the Francevillian Group fossilized structures. Evidence for the early evolution of eukaryotes suggested by the Francevillian Group fossilized structures is at least c. 400 Myrs older than the current undisputed paleontological and organic geochemistry evidence (Gibson et al., 2018; Love et al., 2009; Summons et al., 1988; Pang et al., 2013; Zumberge et al., 2020) and more than 200 Myrs younger than the oldest estimate for the last eukaryote common ancestor (LECA) from molecular clock (Gold et al., 2017; Strassert et al., 2021). Numbers in brackets refer to relevant references: 1 = Gold et al., 2017; 2 = Strassert et al., 2021; 3 = Betts et al., 2018; 4 = Parfrey et al., 2011; 5 = Porter, 2020; 6 = Bengtson et al., 2009; 7 = Pang et al., 2013; 8 = Zhu et al., 2016; 9 = Knoll, 2014; 10 = Knoll et al., 2006; 11 = Gibson et al., 2018; 12 = Love et al., 2009; 13 = Summons et al., 1988; 14 = Zumberge et al., 2020; 15 = Brocks et al., 2017. MC: molecular clock estimate.

such Zn enrichment appears to be typically controlled by biological uptake. Furthermore, when the host rock is enriched in heavy Zn isotopes with respect to fossilized structures, indicating a Zn-replete bioavailable pool, and fossilized structures have high Zn concentrations, several times higher than the host rocks, it is most likely due to a high biological uptake rate of light Zn isotopes by organisms. This particular scenario may point to their eukaryotic rather than prokaryotic affinity. The Francevillian Group fossilized structures are enriched in light Zn isotopes relative to their host rocks, while their Zn concentrations are several times higher than those of their host rocks. These combined geochemical signatures point to a biogenic origin for the Francevillian Group fossilized structures, while enrichment in light Zn isotopes, relative to the bioavailable Zn pool, is consistent with their eukaryotic affinity. Based on these arguments, the Francevillian Group fossilized structures are considered to have eukaryotic affinity. However, since it is not known if negative Zn isotope fractionation is a signature of the whole eukaryotic domain, it is uncertain whether the Francevillian Group fossilized structures represent photosynthetic or non-photosynthetic eukaryotes.

Geochemical evidence presented here also cannot resolve the exact type of eukaryotic organisms that inhabited the Francevillian basin, i.e., colonies of multiple cells or individual, large complex multicellular organisms. By the same token, it remains unconstrained when eukaryotes started to use Zn in metalloenzymes or when Zn-dependent metabolisms became ecologically prominent for the first time. The Zn biogeochemical proxy is however consistent with biological handling of Zn by eukaryotes in marine habitats by at least c. 2.1 Gyrs ago, during the latter part of the GOE.

CRediT authorship contribution statement

Conception and design of the study: Frantz Ossa Ossa and Ronny Schoenberg; **Field sampling:** Frantz Ossa Ossa, Axel Hofmann, Andrey Bekker and Ronny Schoenberg; **Acquisition of data:** Frantz Ossa Ossa, Marie-Laure Pons, Andrea Agangi, Daniel Gregory, Christian Reinke, Bernd Steinhilber, Johanna Marin-Carbonne and Ronny Schoenberg; **Interpretation of data:** Frantz Ossa Ossa

with significant contribution from all authors; **Drafting the article:** Frantz Ossa Ossa; **Revising the article critically for important intellectual content:** Frantz Ossa Ossa, Marie-Laure Pons, Andrey Bekker, Axel Hofmann, Simon W. Poulton, Andrea Agangi, Daniel Gregory, Christian Reinke, Bernd Steinhilber, Johanna Marin-Carbonne and Ronny Schoenberg; **Final approval of the version to be submitted:** Frantz Ossa Ossa, Marie-Laure Pons, Andrey Bekker, Axel Hofmann, Simon W. Poulton, Andrea Agangi, Daniel Gregory, Christian Reinke, Bernd Steinhilber, Johanna Marin-Carbonne and Ronny Schoenberg.

Declaration of competing interest

The authors declare that they have no known competing financial interests or personal relationships that could have appeared to influence the work reported in this paper.

Data availability

All data used in this study are available in the figures and Supplementary material for online publication.

Acknowledgements

thank two anonymous reviewers for thoughtful suggestions and Boswell Wing for editorial handling.

Appendix A. Supplementary material

Supplementary material related to this article can be found online at https://doi.org/10.1016/j.epsl.2023.118147.

References

Anderson, R.P., et al., 2016. Macroscopic structures in the 1.1 Ga Continental Copper Harbor Formation: concretions or fossils? Palaios 31, 37–338.

Andreini, C., Banci, L., Bertini, I., Rosato, A., 2006. Zinc through the three domains of life. J. Proteome Res. 5, 3173–3178.

Arzul, G., Clement, A., Pinier, A., 1996. Effects on phytoplankton growth of dissolved substances produced by fish farming. Aquatic Living Resour. 9, 95–102.

Atiyeh, B.S., Costagliola, M., Hayek, S.N., Dibo, S.A., 2007. Effect of silver on burn wound infection control and healing: review of the literature. Burns 33, 139–148.

Aubineau, J., et al., 2018. Unusual microbial mat-related structural diversity 2.1 billion years ago and implications for the Francevillian biota. Geobiology 16, 476–497.

Bekker, A., El Albani, A., Hofmann, A., Karhu, J.A., Kump, L., Ossa Ossa, F., Planavsky, N.J., 2021. The Paleoproterozoic Francevillian succession of Gabon and the Lomagundi-Jatuli event: Comment. Geology 49 (7), e527.

Bengtson, S., Belivanova, V., Rasmussen, B., Whitehouse, M., 2009. The controversial "Cambrian" fossils of the Vindhyan are real but more than a billion years older. Proc. Natl. Acad. Sci. USA 106, 7729–7734.

Betts, H.C., Puttick, M.N., Clark, J.W., Williams, T.A., Donoghue, P.C.J., Pisani, D., 2018. Integrated genomic and fossil evidence illuminates life's early evolution and eukaryote origin. Nat. Ecol. Evol. 2, 1556–1562.

Boxall, A., Chaudhry, Q., Sinclair, C., Jones, A., Jefferson, B., Watts, C., 2007. Current and Future Predicted Environmental Exposure to Engineered Nanoparticles. CSL, York, UK.

Brocklehurst, K.R., et al., 1999. ZntR is a Zn(II)-responsive MerR-like transcriptional regulator of zntA in Escherichia coli. Mol. Microbiol. 31, 893–902.

Brocks, J.J., et al., 2017. The rise of algae in Cryogenian oceans and the emergence of animals. Nature 548, 578–581.

Burki, F., Roger, A.J., Brown, M.W., Simpson, A.G.B., 2020. The new tree of eukaryotes. Trends Ecol. Evol. 35, 43–55.

Butterfield, N.J., 2015. Early evolution of the Eukaryota. Palaeontology 58, 5–17.

Costello, L.C., Franklin, R.B., 1998. Novel role of zinc in the regulation of prostate citrate metabolism and its implications in prostate cancer. Prostate 35, 285–296.

Costello, L.C., Guan, Z., Franklin, R.B., Feng, P., 2004. Metallothionein can function as a chaperone for zinc uptake transport into prostate and liver mitochondria. J. Inorg. Biochem. 98, 664–666.

Dedman, C.J., Newson, G.C., Davies, G-L., Christie-Oleza, J.A., 2020. Mechanisms of silver nanoparticle toxicity on the marine cyanobacterium Prochlorococcus under environmentally relevant conditions. Sci. Total Environ. 747, 141229.

Duong, T.T., et al., 2016. Inhibition effect of engineered silver nanoparticles to bloom forming cyanobacteria. Adv. Nat. Sci: Nanosci. Nanotechnol. 7, 035018.

Dupont, C.L., Butcher, A., Valas, R.E., Bourne, P.E., Caetano-Anollés, G., 2010. History of biological metal utilization inferred through phylogenomic analysis of protein structures. Proc. Natl. Acad. Sci. USA 107, 10567–10572.

Eide, D.J., 2003. Multiple regulatory mechanisms maintain zinc homeostasis in Saccharomyces cerevisiae. J. Nutr. 133, 532S–1535S.

Eide, D.J., 2006. Zinc transporters and the cellular trafficking of zinc. Biochim. Biophys. Acta 1763, 711–722.

Eisler, R., 2009. In: Eisler, Ronald (Ed.), Compendium of Trace Metals and Marine Biota, vol. 2.

El Albani, A., et al., 2010. Large colonial organisms with coordinated growth in oxygenated environments 2.1 Gyr ago. Nature 466, 100–104.

El Albani, A., et al., 2014. The 2.1 Ga old Francevillian biota: biogenicity, taphonomy and biodiversity. PLoS ONE 9, e99438.

El Albani, A., et al., 2019. Organism motility in an oxygenated shallow-marine environment 2.1 billion years ago. Proc. Natl. Acad. Sci. USA 116, 3431–3436.

Eme, L., Sharpe, S.C., Brown, M.W., Roger, A.J., 2014. On the age of eukaryotes: evaluating evidence from fossils and molecular clocks. Cold Spring Harb. Perspect. Biol. 6, a016139.

Fujii, T., Moynier, F., Pons, M-L., Albarède, F., 2011. The origin of Zn isotope fractionation in sulfides. Geochim. Cosmochim. Acta 75, 7632–7643.

Gauthier-Lafaye, F., Weber, F., 2003. Natural nuclear fission reactors: time constraints for occurrence, and their relation to uranium and manganese deposits and to the evolution of the atmosphere. Precambrian Res. 120, 81–100.

Gibson, T.M., et al., 2018. Precise age of Bangiomorpha pubescens dates the origin of eukaryotic photosynthesis. Geology 46, 135–138.

Gold, D.A., Caron, A., Fournier, G.P., Summons, R.E., 2017. Paleoproterozoic sterol biosynthesis and the rise of oxygen. Nature 543, 420–423.

Hawco, N.J., Saito, M.A., 2018. Competitive inhibition of cobalt uptake by zinc and manganese in a pacific Prochlorococcus strain: Insights into metal homeostasis in a streamlined oligotrophic cyanobacterium. Limnol. Oceanogr. 63, 2229–2249.

Hu, S-Y., et al., 2018. Sequestration of Zn into mixed pyrite-zinc sulfide framboids: a key to Zn cycling in the ocean? Geochim. Cosmochim. Acta 241, 95–107.

Huertas, M.J., et al., 2014. Metals in Cyanobacteria: analysis of the copper, nickel, cobalt and arsenic homeostasis mechanisms. Life 4, 865–886.

Inoue, J., Donoghue, P.C.J., Yang, Z., 2010. The impact of the representation of fossil calibrations on Bayesian estimation of species divergence times. Syst. Biol. 59, 74–89.

Javaux, E.J., 2019. Challenges in evidencing the earliest traces of life. Nature 572, 451–460.

John, S.G., Geis, R.W., Saito, M.A., Boyle, E.A., 2007. Zinc isotope fractionation during high-affinity and low-affinity zinc transport by the marine diatom Thalassiosira oceanica. Limnol. Oceanogr. 52, 2710–2714.

John, S.G., Rouxel, O.J., Craddock, P.R., Engwall, A.M., Boyle, E.A., 2008. Zinc stable isotopes in seafloor hydrothermal vent fluids and chimneys. Earth Planet. Sci. Lett. 269, 17–28.

Kadukova, J., 2016. Surface sorption and nanoparticle production as a silver detoxification mechanism of the freshwater alga Parachlorella kessleri. Bioresour. Technol. 216, 406–413.

Karhu, J.A., Holland, H.D., 1996. Carbon isotopes and the rise of atmospheric oxygen. Geology 24, 867–870.

Knoll, A.H., 2014. Paleobiological perspectives on early eukaryotic evolution. Cold Spring Harb. Perspect. Biol. 6, a016121.

Knoll, A.H., Javaux, E.J., Hewitt, D., Cohen, P., 2006. Eukaryotic organisms in Proterozoic oceans. Philos. Trans. R. Soc. Lond. B, Biol. Sci. 361, 1023–1038.

Köbberich, M., Vance, D., 2019. Zn isotope fractionation during uptake into marine phytoplankton: implications for oceanic zinc isotopes. Chem. Geol. 523, 154–161.

Large, R.R., et al., 2014. Trace element content of sedimentary pyrite as a new proxy for deep-time ocean–atmosphere evolution. Earth Planet. Sci. Lett. 389, 209–220.

Little, S.H., Vance, D., Walker-Brown, C., Landing, W.M., 2014. The oceanic mass balance of copper and zinc isotopes, investigated by analysis of their inputs, and outputs to ferromanganese oxide sediments. Geochim. Cosmochim. Acta 125, 673–693.

Little, S.H., Vance, D., McManus, J., Severmann, S., 2016. Key role of continental margin sediments in the oceanic mass balance of Zn and Zn isotopes. Geology 44, 207–210.

Love, G.D., et al., 2009. Fossil steroids record the appearance of Demospongiae during the Cryogenian period. Nature 457, 718–721.

Malysheva, A., Ivask, A., Doolette, C.L., Voelcker, N.H., Lombi, E., 2021. Cellular binding, uptake and biotransformation of silver nanoparticles in human T lymphocytes. Nat. Nanotechnol. 16, 926–932.

Morel, F.M.M., Reinfelder, J.R., Roberts, S.B., Chamberlain, C.P., Lee, J.G., Yee, D., 1994. Zinc and carbon co-limitation of marine phytoplankton. Nature 369, 740–742.

Nasir, M.S., Fahrni, C.J., Suhy, D.A., Kolodsick, K.J., Singer, C.P., O'Halloran, T.V., 1999. The chemical cell biology of zinc: structure and intracellular fluorescence of a zinc–quinolinesulfonamide complex. J. Biol. Inorg. Chem. 4, 775–783.

Nelson, L.L., Smith, E.F., 2019. Tubey or not tubey: death beds of Ediacaran macrofossils or microbially induced sedimentary structures? Geology 47, 909–913.

Ossa Ossa, F., et al., 2013. Exceptional preservation of expandable clay minerals in the ca. 2.1 Ga black shales of the Francevillian basin, Gabon and its implication for atmospheric oxygen accumulation. Chem. Geol. 362, 181–192.

Ossa Ossa, F., et al., 2018. Two-step deoxygenation at the end of the Paleoproterozoic Lomagundi event. Earth Planet. Sci. Lett. 486, 70–83.

Ossa Ossa, F., et al., 2022. Moderate levels of oxygenation during the late stage of Earth's Great Oxidation event. Earth Planet. Sci. Lett. 594, 117716. https://doi.org/10.1016/j.epsl.2022.117716.

Outten, C.E., O'Halloran, T.V., 2001. Femtomolar sensitivity of metalloregulatory proteins controlling zinc homeostasis. Science 292, 2488–2492.

Pang, K., et al., 2013. The nature and origin of nucleus like intracellular inclusions in Paleoproterozoic eukaryote microfossils. Geobiology 11, 499–510.

Patzer, S.I., Hantke, K., 1998. The ZnuABC high affinity zinc uptake system and its regulator Zur in Escherichia coli. Mol. Microbiol. 28, 1199–1210.

Parfrey, L.W., Lahr, D.J.G., Knoll, A.H., Katz, L.A., 2011. Estimating the timing of early eukaryotic diversification with multigene molecular clocks. Proc. Natl. Acad. Sci. USA 108, 13624–13629.

Perez, J.L., Chu, T., 2020. Effect of zinc on Microcystis aeruginosa UTEX LB 2385 and its toxin production. Toxins 12, 92.

Porter, S.M., 2020. Insights into eukaryogenesis from the fossil record. Interface Focus 10, 20190105. https://doi.org/10.1098/rsfs.2019.0105.

Prave, A.R., et al., 2021. The grandest of them all: the Lomagundi–Jatuli event and Earth's oxygenation. J. Geol. Soc. 179. https://doi.org/10.1144/jgs2021-03.

Qian, H., et al., 2016. Contrasting silver nanoparticle toxicity and detoxification strategies in Microcystis aeruginosa and Chlorella vulgaris: new insights from proteomic and physiological analyses. Sci. Total Environ. 572, 1213–1221.

Ramsay, L.M., Gadd, G.M., 1997. Mutants of Saccharomyces cerevisiae defective in vacuolar function confirm a role for the vacuole in toxic metal ion detoxification. FEMS Microbiol. Lett. 152, 293–298.

Rudnick, R.L., Gao, S., 2014. Composition of continental crust. In: Holland, H.D., Turekian, K.K. (Eds.), In: Treatise on Geochemistry, vol. 4, pp. 1–51.

Samanta, M., Ellwood, M.J., Strzepek, R.F., 2018. Zinc isotope fractionation by *Emiliania huxleyi* cultured across a range of free zinc ion concentrations. Limnol. Oceanogr. 63, 660–671.

Seilacher, A., 2001. Concretion morphologies reflecting diagenetic and epigenetic pathways. Sediment. Geol. 143, 41–57.

Shaked, Y., Xu, Y., Leblanc, K., Morel, F.M.M., 2006. Zinc availability and alkaline phosphatase activity in Emiliania huxleyi: implications for Zn-P co-limitation in the ocean. Limnol. Oceanogr. 51, 299–309.

Strassert, J.F.H., Irisarri, I., Williams, T.A., Burki, F., 2021. A molecular timescale for eukaryote evolution with implications for the origin of red algal-derived plastids. Nat. Commun. 12, 1879. https://doi.org/10.1038/s41467-021-23847-w.

Summons, R.E., et al., 1988. Distinctive hydrocarbon biomarkers from fossiliferous sediments of the Late Proterozoic Walcott Member, Chuar Group, Grand Canyon, Arizona. Geochim. Cosmochim. Acta 52, 2625–2637.

Vallee, B.L., Falchuk, K.H., 1993. The biochemical basis of zinc physiology. Physiol. Rev. 73, 79–118.

Vance, D., et al., 2016. The oceanic budgets of nickel and zinc isotopes: the importance of sulphidic environments as illustrated by the Black Sea. Philos. Trans. R. Soc. Lond. Ser. A 374, 20150294.

Viers, J., et al., 2007. Evidence of Zn isotopic frationation in a soil–plant system of a pristine tropical watershed (Nsimi, Cameroon). Chem. Geol. 239, 124–137.

Wang, S., Lv, J., Ma, J., Zhang, S., 2016. Cellular internalization and intracellular biotransformation of silver nanoparticles in Chlamydomonas reinhardti. Nanotoxicology 10, 1129–1135.

Weiss, D.J., Mason, T.F.D., Zhao, F.J., Kirk, G.J.D., Coles, B.J., Horstwood, M.S.A., 2005. Isotopic discrimination of zinc in higher plants. New Phytol. 165, 703–710.

Wilkinson, J.J., Weiss, D.J., Mason, T.F.D., Coles, B.J., 2005. Zinc isotope variation in hydrothermal systems: preliminary evidence from the Irish Midlands ore field. Econ. Geol. 100, 583–590.

Zhang, X., Zhai, S., Yu, Z., Yang, Z., Xu, J., 2019. Zinc and lead isotope variation in hydrothermal deposits from the Okinawa Trough. Ore Geol. Rev. 111, 102944. https://doi.org/10.1016/j.oregeorev.2019.102944.

Zhu, S., et al., 2016. Decimetre-scale multicellular eukaryotes from the 1.56-billion-year-old Gaoyuzhuang Formation in North China. Nat. Commun. 7, 11500.

Zumberge, J.A., Rocher, D., Love, G.D., 2020. Free and kerogen-bound biomarkers from late Tonian sedimentary rocks record abundant eukaryotes in mid-Neoproterozoic marine communities. Geobiology 18, 326–347.